Second and third order susceptibilities mixing for supercontinuum generation and shaping

Fabio Baronio, Matteo Conforti, Costantino de Angelis, Daniele Modotto, Stefan Wabnitz, Marco Andreana, Alessandro Tonello, Philippe Leproux, Vincent Couderc

Second and third order susceptibilities mixing for supercontinuum generation and shaping

Fabio Baronio[a,*], Matteo Conforti[a], Costantino De Angelis[a], Daniele Modotto[b], Stefan Wabnitz[b], Marco Andreana[c], Alessandro Tonello[c], Philippe Leproux[c], Vincent Couderc[c]

[a] *CNISM and Dipartimento di Ingegneria dell'Informazione, Università degli Studi di Brescia, via Branze 38, 25123, Brescia, Italy*
[b] *CNIT and Dipartimento di Ingegneria dell'Informazione, Università degli Studi di Brescia, via Branze 38, 25123, Brescia, Italy*
[c] *XLIM UMR CNRS 7252, Université de Limoges, 123 av. Albert Thomas, 87060 Limoges, France*

Abstract

We report our recent development to model quadratic and cubic ultra-broadband nonlinear dynamics in photonic devices, by means of a nonlinear single-envelope equation. We present the case of generation of tunable visible light from large band conversion, in a quadratic crystal, of the infrared continuum from standard photonic crystal fibers. Moreover, we show the study of a visible supercontinuum generation, initiated by second-harmonic generation, in a quadratic poled germanium-doped microstructured fiber.

Keywords: nonlinear optics, supercontinuum, microstructured optical fiber

*Corresponding author
Email address: baronio@ing.unibs.it (Fabio Baronio)

1. Introduction

There is considerable interest in developing robust and compact optical frequency sources in the ultraviolet (UV), visible, infrared (IR) and mid-infrared (MIR, i.e. from $2 - 12\mu m$) spectral regions for spectroscopy, coherence tomography, frequency metrology, few-cycle pulse generation, optical sensing, and material processing. Nonlinear optical processes are usually required to generate frequencies in regions not directly accessible through well-developed broadband laser gain media. Spectral generation of new frequency components is a inherent feature of nonlinear optics, and has been studied intensively since the early $1960s$ [1]. In this context, several promising methods have been considered, including optical parametric oscillators (OPOs) [2, 3], difference frequency generation (DFG) [4, 5, 6], and supercontinuum (SC) generation [7, 8, 9, 10].

The particular process known as SC generation occurs when narrow-band incident pulses undergo extreme nonlinear spectral broadening to yield a broadband spectrally continuous output. First reported in bulk glasses [11], SC has since been the subject of numerous investigations in a wide variety of cubic nonlinear media, including solids, organic and inorganic liquids, gases, and various type of waveguides. The advent of a new class of optical waveguides in the form of a photonic crystal fiber (PCF) in the late $1990s$ has attracted widespread interest throughout the scientific community, and led to a revolution in the generation of ultrabroadband high brightness spectra through SC generation [12, 13, 14]. SC PCF generation has already found numerous applications in such diverse fields as spectroscopy, pulse compression, and the design of tunable ultrafast femtosecond laser sources. In a

telecommunications context, the spectral slicing of broadband SC spectra has also been proposed as a simple way to create multiwavelength optical sources for dense wavelength division multiplexing applications.

SC PCFs are designed to provide a flat spectrum over a wide wavelength range, but the produced spectrum is directly dependent on parameters such as fiber material and structure, fiber length, pump power, pump wavelength. In spite of the great flexibility in generating such a wide range of wavelengths, it is not already demonstrated the possibility to synthetise a well defined amplitude and phase profile of the SC spectrum directly by designing the fiber or other system parameters.

A general and extremely flexible option for reaching wavelengths which are difficult to obtain by employing cubic nonlinearities, or for shaping the spectrum of PCF sources, could be provided by exploiting a mixture of quadratic and cubic effects. In fact, quadratic nonlinear materials can be properly engineered to generate, with high-efficiency, pulses with transform limited duration, predetermined spectral and temporal shapes, and synchronization [15, 16, 17]. Examples of the synthesis of super-Gaussian pulses and of pairs of phase-coherent picosecond pulses with a given carrier-frequency detuning, by designing aperiodically poled quadratic ferroelectric domains, were recently given in Ref. [18, 19].

In this paper, we report our recent developments in the study of broadband quadratic and cubic interactions. The paper is organized as follows: in Section 2 we introduce a single-envelope model to capture ultra-broadband interactions in quadratic and cubic nonlinear media. Our equation, besides providing a simple and powerful tool for analytical treatment due to its sim-

plicity, can be easily solved with a modest computational effort. The only alternative way to numerically describe ultrabroadband quadratic and cubic phenomena is to solve directly Maxwell equations in the time domain, with an immense computational burden. Section 3 reports the case of tunable light sources from large band conversion of PCF continuum by quadratic crystals. Section 4 considers the SC visible generation, initiated by second-harmonic generation, in quadratic poled germanium-doped PCFs. Conclusions appear in Section 5.

2. Single-envelope model for broadband interactions

Starting from Maxwell equations (written in MKS units), neglecting transverse dimensions (i.e considering the propagation of plane waves in bulk media or bound modes in waveguides), we can write the 1+1D wave equation for the electric field $E(z,t)$ [20]:

$$\frac{\partial^2 E(z,t)}{\partial z^2} - \frac{1}{c^2}\frac{\partial^2}{\partial t^2}\int_{-\infty}^{+\infty} E(z,t')\varepsilon(t-t')dt' = \frac{1}{\varepsilon_0 c^2}\frac{\partial^2}{\partial t^2}P_{NL}(z,t). \qquad (1)$$

By defining the Fourier transform $\mathcal{F}[E](\omega) = \hat{E}(\omega) = \int_{-\infty}^{+\infty} E(t)e^{-i\omega t}dt$, we can write (1) in frequency domain:

$$\frac{\partial^2 \hat{E}(z,\omega)}{\partial z^2} + \frac{\omega^2}{c^2}\hat{\varepsilon}(\omega)\hat{E}(z,\omega) = -\frac{\omega^2}{\varepsilon_0 c^2}\hat{P}_{NL}(z,\omega), \qquad (2)$$

where c is the velocity of light in vacuum, ε_0 is the vacuum dielectric permittivity, $\hat{\varepsilon}(\omega) = 1 + \hat{\chi}(\omega)$, $\hat{\chi}(\omega)$ is the linear electric susceptibility and $k(\omega) = (\omega/c)\sqrt{\hat{\varepsilon}(\omega)}$ is the propagation constant. In the case of waveguides, $k(\omega)$ is the wavenumber of the propagating mode. We now factor out the fast dependence of the propagation coordinate from the electric field, for all frequencies: $\hat{E}(z,\omega) = \hat{U}(z,\omega)\exp[-ik(\omega)z]$ [21]. This definition amounts to

write the electric field as the product of a spatial carrier wave and a slowly varying envelope. Since we remove the exact propagation constant at every frequency, we can avoid to make a requirement on the bandwidth of the pulses. The wave equation for the field $\hat{U}$ reads as:

$$\frac{\partial^2 \hat{U}(z,\omega)}{\partial z^2} - 2ik(\omega)\frac{\partial \hat{U}(z,\omega)}{\partial z} = -\frac{\omega^2}{\varepsilon_0 c^2}\hat{P}_{NL}(z,\omega)e^{ik(\omega)z}. \tag{3}$$

We make the slowly evolving wave approximation (SEWA) [21], that is $|\partial_z \hat{U}| << 2k(\omega)|\hat{U}|$, and thus we can write

$$\frac{\partial \hat{U}(z,\omega)}{\partial z} = -i\frac{\omega^2}{2\varepsilon_0 c^2 k(\omega)}\hat{P}_{NL}(z,\omega)e^{ik(\omega)z}, \tag{4}$$

and from the definition of $\hat{U}$, we obtain the equation for the electric field:

$$\frac{\partial \hat{E}(z,\omega)}{\partial z} + ik(\omega)\hat{E}(z,\omega) = -i\frac{\omega}{2\varepsilon_0 c n(\omega)}\hat{P}_{NL}(z,\omega). \tag{5}$$

This equation has been found by an heuristic method, and has been termed Forward Maxwell Equation (FME) [22]. Once specified the form of nonlinearity, we can directly solve Eq.(5) in frequency domain with a standard split-step Fourier method. When backward waves can be neglected, this equation is equivalent to Maxwell equations [22, 23], but the numerical solution is much more efficient.

However, we can simplify further Eq. (5) by properly defining an envelope. We consider the electric field E and the nonlinear polarization P_{NL} as the product of a complex envelope and a carrier wave:

$$E(z,t) = \frac{1}{2}A(z,t)e^{i\omega_0 t - i\beta_0 z} + c.c., \tag{6}$$

$$P_{NL}(z,t) = \frac{1}{2}A_p(z,t)e^{i\omega_0 t - i\beta_0 z} + c.c, \tag{7}$$

that in frequency domain reads:

$$\begin{aligned}\hat{E}(z,\omega) &= \frac{1}{2}\hat{A}(z,\omega-\omega_0)e^{-i\beta_0 z}+\frac{1}{2}\hat{A}^*(z,-\omega-\omega_0)e^{i\beta_0 z},\\ \hat{P}_{NL}(z,\omega) &= \frac{1}{2}\hat{A}_p(z,\omega-\omega_0)e^{-i\beta_0 z}+\frac{1}{2}\hat{A}_p^*(z,-\omega-\omega_0)e^{i\beta_0 z},\end{aligned}$$

where ω_0 is a reference frequency, $\beta_0 = Re[k(\omega_0)]$. Particular care must be devoted to the definition of the complex envelope, since we do not want to impose any limitation to the frequency extent of the signals. For nonlinear media, a proper definition of the envelope is crucial [24, 25]. As usual in the theory of modulation [26], we define the analytic representation of the electric field:

$$\tilde{E}(z,t) = E(z,t) + i\mathcal{H}[E](z,t), \tag{8}$$

where

$$\mathcal{H}[E](z,t) = \frac{1}{\pi} p.v. \int_{-\infty}^{+\infty} \frac{E(z,t')}{t-t'} dt' \tag{9}$$

is the Hilbert transform of the electric field ($p.v.$ indicates the Cauchy principal value of the integral). The Fourier transform of the analytic signal reads:

$$\hat{\tilde{E}}(z,\omega) = \begin{cases} 2\hat{E}(z,\omega) & \text{if } \omega > 0 \\ \hat{E}(z,0) & \text{if } \omega = 0 \\ 0 & \text{if } \omega < 0 \end{cases}, \tag{10}$$

that is a signal that contains only the positive frequency content of the electric field. Due to reality of $E(z,t)$, its Fourier transform has Hermitian symmetry, so that only the positive (or the negative) frequencies carry information, and we can write:

$$\hat{E}(z,\omega) = \frac{1}{2}\hat{\tilde{E}}(z,\omega) + \frac{1}{2}\hat{\tilde{E}}^*(z,-\omega), \tag{11}$$

we can define the complex electric field envelope (6) as:

$$A(z,t) = \tilde{E}(z,t)e^{-i\omega_0 t + i\beta_0 z}, \tag{12}$$

i.e. the inverse Fourier transform of the positive frequency content of E shifted towards the low frequency part of the spectrum by an amount ω_0. No approximations on the frequency extent of the envelope has been done, and $\mathrm{supp}\{\hat{A}(z,\omega)\} = (-\omega_0, +\infty)$.

The substitution of expressions of $\hat{E}(z,\omega)$ and $\hat{P}_{NL}(z,\omega)$ in Eq. (5) and the Taylor-expansion of $k(\omega)$ about ω_0 yields:

$$\frac{\partial \hat{A}(z,\Omega)}{\partial z} + i\Big[\sum_{m=1}^{\infty} \frac{k_m}{m!}\Omega^m\Big]\hat{A}(z,\Omega) = -i\frac{\omega}{2n(\omega)c\varepsilon_0}\hat{A}_p(z,\Omega), \tag{13}$$

where $\Omega = \omega - \omega_0$ and $k_m = \frac{\partial^m k}{\partial \omega^m}(\omega_0)$. In order to obtain a time domain equation we have to perform another approximation, i.e. we have to impose that $n(\omega)$ is nearly constant in the frequency band of interest. Since we want to take into account ultra-broad spectra, we require the validity of this condition on a band whose order of magnitude is the same of the carrier frequency, that is $\frac{\partial n(\omega)}{\partial \omega}|_{\omega_0}\omega_0 << n(\omega_0)$. Far from resonances, this requirement is fulfilled in the majority of parametric processes in which all waves propagate in the same direction. By inverse Fourier transform we obtain from (13)

$$\frac{\partial A(z,t)}{\partial z} + iD'A(z,t) = -i\frac{\omega_0}{2n_0 c\varepsilon_0}\Big(1 - \frac{i}{\omega_0}\frac{\partial}{\partial t}\Big)A_p(z,t), \tag{14}$$

where we have defined the dispersive operator $D' = \sum_{m=1}^{\infty} \frac{1}{m!}k_m(-i\frac{\partial}{\partial t})^m$.

As a last step, we consider quadratic and cubic nonlinearities, in particular the following nonlinear polarization:

$$P_{NL}(z,t) \;=\; P_{NL}^{(2)}(z,t) + P_{NL}^{(3)}(z,t) \tag{15}$$

$$= \varepsilon_0\chi^{(2)}E(z,t)^2 + \varepsilon_0\chi^{(3)}E(z,t)\int R(t-t')|E(z,t')|^2dt'. \quad (16)$$

where the causal $R(t) = (1-f_r)\delta(t) + f_r h_r(t)$ includes both instantaneous electronic and delayed Raman contributions [7]. The integrals are in the range $(-\infty, +\infty)$. As to quadratic nonlinearity,

$$\begin{aligned} P^{(2)}_{NL}(z,t) &= \varepsilon_0\chi^{(2)}E(z,t)^2 \\ &= \frac{\varepsilon_0\chi^{(2)}}{4}\Big[A^2e^{2i\omega_0t-2i\beta_0z} + A^{*2}e^{-2i\omega_0t+2i\beta_0z} + 2|A|^2\Big]. \end{aligned}$$

It is worth noting that, due to the definition of A, the first (second) term in the square brackets contains only positive (negative) frequencies, whereas the third has both. By going through the steps (8)-(12) we can define the quadratic nonlinear polarization envelope [24, 25]:

$$\begin{aligned} A^{(2)}_p(z,t) &= \tilde{P}^{(2)}_{NL}(z,t)e^{-i\omega_0t+i\beta_0z} \\ &= \frac{\varepsilon_0\chi^{(2)}}{2}\Big[A^2e^{i\omega_0t-i\beta_0z} + \Big(|A|^2 + i\mathcal{H}[|A^2|]\Big)e^{-i\omega_0t+i\beta_0z}\Big] \quad (17) \end{aligned}$$

Before inserting Eq. (17) into Eq. (14), the term $|A|^2$ in Eqs. (17) deserves further comments, since it is centered around zero in frequency domain. In particular to obtain the nonlinear polarization envelope in Eq. (17) we had to filter out the negative frequency components of $\hat{P}_{NL}(\omega)$, as done for $\hat{E}(\omega)$. We note however that (i) $\hat{A}(z, \omega-\omega_0)$ does not contain negative frequency by definition, (ii) P_{NL} is a small perturbation to the linear polarization and (iii) negative frequencies cannot be phase-matched. It follows that the task of filtering the negative frequency components of $|A|^2$ can be left to the propagation equation instead of having it explicitly in the definition of $A^{(2)}_p(z,t)$. In other words, when inserting Eq. (17) into Eq. (14), we

can write: $|A|^2 + i\mathcal{H}[|A^2|] \approx 2|A|^2$. We have checked numerically the good accuracy of this approximation. Even if this approximation in not necessary in the numerical solution (it is straightforward to calculate the exact nonlinear polarization envelope in frequency domain), it is suitable to obtain a simple and manageable model for further analytical investigations [27].

As to cubic nonlinearity,

$$P_{NL}^{(3)}(z,t) \;=\; \varepsilon_0 \chi^{(3)} E(z,t) \int R(t-t')|E(z,t')|^2 dt' \tag{18}$$

and, after some algebra through the steps (8)-(12), we obtain

$$\begin{aligned} A_p^{(3)}(z,t) \;&=\; \frac{\varepsilon_0 \chi^{(3)}}{2} A(z,t) \int dt' R(t')|A(z,t-t')|^2 + \\ &+\; \frac{\varepsilon_0 \chi^{(3)}}{4} A^*(z,t) \int dt' R(t') A^2(z,t-t') e^{-2i\omega_0 t'} + \\ &+\; \frac{\varepsilon_0 \chi^{(3)}}{4} A e^{2i\omega_0 t - 2i\beta_0 z} \int dt' R(t') A^2(z,t-t') e^{-2i\omega_0 t'}. \end{aligned} \tag{19}$$

.

Examples of numerical solutions of Eqs.(14)–(17) (but neglecting the Raman contribution) for describing harmonic wave and supercontinuum generation in quadratic and cubic nonlinear crystals were reported in Ref.[28]. The method reported above can be extended to the case of several propagating modes [29] and different electric field polarizations [30].

3. Infrared PCF supercontinuum and quadratic crystals

As mentioned, supercontinuum light generation in PCF has been developed very successfully during recent decades as a powerful concept for wideband fiber light sources. It relies on cubic nonlinear effects such as four-wave

mixing, soliton propagation, cross-phase modulation and Raman conversion. Efficient supercontinuum light generation requires a suitable design of the dispersion relationship of the fiber. Microstructured PCFs offer new and flexible ways to manipulate the light generation process. Special glasses with high nonlinearity can also be used in the fiber core region [31]. By changing the structure of the cladding, the linear and nonlinear properties of the PCF can be adapted for pumping with different sources in order to generate the targeted wavelength ranges. In silica PCFs, numerous studies have demonstrated SC generation covering a wavelength range from UV (around $400nm$) to near-IR ($2.2\mu m$) [32]. By replacing the silica with other glasses such as tellurite or heavy oxide SF-57 glasses [33], the SC spectrum is shifted towards the higher infrared wavelengths up to about $4\mu m$.

In spite of the great flexibility in generating such a wide range of wavelengths, the possibility to achieve a specific wavelength spectrum directly by designing the fiber or other system parameters is not already demonstrated. A single-pass frequency doubler device may convert the SC broadband infrared radiation into visible light with a tunable carrier wavelength, desired temporal durations, and good-efficiency conversion [15, 16, 17]. To this end, we can expoit the nonlinear envelope technique, introduced in Sec. 2, to simulate the dynamics of a SC PCF infrared radiation injected in a quadratic crystal and to guide experiments of frequency conversion.

For a demonstration experiment, the setup depicted in Fig. 1 is employed. A passively Q–switched Nd:YAG laser delivering $800ps$ pulses at $1064nm$ is used as a pump source. The repetition rate and the peak power were $8kHz$ and $10kW$, respectively. Two half wave plates and a polarizer allowed to

control the power and polarization direction of pump radiation. The pump is coupled into a PCF by an aspheric lens with a coupling efficiency of 75%. For fiber supercontinuum generation, we used a PCF with a core diameter of $4.2\mu m$ whereas the hole diameter and the hole-to-hole spacing are $2.5\mu m$ and $4\mu m$ respectively (Fig. 2). The zero dispersion wavelength for the fundamental guided mode is located close to $990nm$ (Fig. 2), and the mode effective area is about $3.6\mu m^2$ at 1064 nm. The nonlinear refrative index is $2.7 \cdot 10^{-20} m^2 W^{-1}$. By coupling the pump radiation into a $8m$ long fiber in the anomalous dispersion regime, we generated a broadband spectrum mainly extending in the infrared domain, induced by the combination of modulational instability, solitonic propagation and cross-phase modulation effects. Fig. 3 reports a typical experimental SC spectrum at the output of the PCF, characterized by an optical spectrum analyzer (OSA), and the spectrum obtained through numerical simulations, averaged over 30 measurements to mimic the integration time of the OSA. After the propagation through a spectral filter (FEL1000) in order to remove any noise in the 400nm-800 nm band, the SC extended in the IR range $(1064 - 2220nm)$ with an average power of $50mW$. We considered a compact SC system with a wide wavelength range, which can be easily manipulated externally.

The SC is then focused onto a $2cm$ long quadratic biaxial LBO crystal, at the temperature $T = 27^oC$. As an example, we show the case of light propagation in the principal plane XY of the biaxial crystal with the azimuthal angle ϕ varying from 0^o to 5^o. The spectra were subsequently characterized by the OSA. Fig. 4 reports a typical experimental spectrum at the output of the quadratic LBO crystal, and the spectrum obtained through broadband nu-

merical simulations. In fact, second harmonic generation (SHG) takes place in the quadratic crystal, generating wavelengths in the visible band. Fig. 5 reports typical temporal profiles of signals generated in the visible range. The wavelengths of the waves can be tuned by simply varying the azimuthal angle of the LBO crystal. Fig. 6 reports experimental visible spectra at the output of the quadratic LBO crystal, at different azimuthal crystal angle ϕ. At $\phi = 0$, a $100nm$ width spectrum in the visible domain is generated. Fig. 6 also shows the theoretical contour plots of the normalised parametric gain for second harmonic generation varying the crystal azimuthal angle (the curves are calculated from Sellmeier equations for LBO at temperature $T = 27^o$ C).

Reverse engineering [15] through the nonlinear envelope equation could allow one to choose different crystals permitting the generation of waves in different regions of the spectrum and/or with desired temporal durations. As an example, the combination of a PCF designed for broadband SC generation in the visible and a KDP crystal would lead to the generation of fields in the UV spectrum.

4. Visible supercontinuum in optically poled PCFs

For many biomedical applications, it would be highly desirable to have a fiber-based broadband, high-brightness source of light in the visible range of the spectrum. An approach to generate visible optical SC is to use a tapered PCF, where the zero-dispersion wavelength, initially located close to the pump wavelength at, e.g., $800nm$, is gradually shifted towards shorter wavelengths [34]. As we saw in the previous section, a different approach to visible SC generation may involves the frequency doubling of the infrared SC by means of a quadratic crystal. Alternatively, visible SC may be directly

generated in the fiber itself by exploiting its cubic and quadratic nonlinear response.

Although the second-order order susceptibility is not present in silica because of centrosimmetry, several experiments have indeed reported SHG in germanium-doped silica fibers, due to either dipolar effects at the core-cladding interface [35], or to a cascading process involving the third-order nonlinearity mediated creation, from an initial doping-induced weak SHG, of a static electric field which induces a grating for quasi-phase-matching [36]. In all of these experiments, the SHG efficiency was not sufficient to lead to visible SC generation when the fiber was pumped by an infrared beam. In 2004, a method for visible SC generation was investigated by several research teams [37]. The method consists of the double excitation of a PCF by launching an IR radiation ($1064nm$) and its second harmonic ($532nm$), the latter being generated through a nonlinear crystal. A spectral broadening is obtained in the IR domain by means of solitonic effects, whereas the visible spectrum is induced by the cross-phase modulation (XPM) of the IR solitons on the harmonic pump wave. In that way, a significant visible spectrum enlargement can be obtained for any value of the second-harmonic (SH) power, even weak, its spectral width being determined by the IR radiations velocities. It was also demonstrated that the dual pumping process writes a permanent grating in the germanium-doped fiber, so that efficient broadband SHG can be obtained directly from the poled fiber when using the IR pump only [38]. Recent experiments have investigated the limitations due to the Raman effect in the self-poling process occurring in a germanium-doped standard single-mode fiber [39].

Here, we consider and model the case of SC visible generation, initiated by second-harmonic generation, in quadratic poled germanium-doped PCFs [38]. A passively Q–switched Nd:YAG laser delivering $650ps$ pulses at $1064nm$ is used as a pump source. The repetition rate and the peak power were $12.5kHz$ and $2.5kW$, respectively. The pump is coupled into a $4m$-long germanium-doped PCF. For fiber supercontinuum generation, we used a PCF with a core diameter of $1.8\mu m$ whereas the average hole diameter is $2.1\mu m$ and the pitch is $2.3\mu m$ (Fig. 7). The zero dispersion wavelength for the fundamental guided mode is located close to $875nm$ (Fig. 7), and the mode effective area is about $2.4\mu m^2$ at 1064 nm. The nonlinear refrative index is $2.6{\cdot}10^{-20}m^2W^{-1}$. The PCF has been previously poled by both green ($532nm$) and IR ($1064nm$) radiation beating. In the first $45cm$ of the PCF, a quadratic square spatial modulation is estimated, with $0.001pm/V$ magnitude and $\Lambda = 25.8\mu m$ grating period, respectively.

By coupling the pump radiation at $1064nm$ into the poled PCF, a broadband IR SC is produced by Raman self-frequency shifting solitons accompanied by a lower amplitude, visible and symmetric XPM-induced SC, extending over about $200nm$ around $532nm$. Fig. 8 reports a typical experimental spectrum at the output of the PCF, characterized by the OSA. Fig. 9 reports the spectrum obtained through numerical simulations. Fig. 9 illustrates the numerical spectra at different lengths of the PCF, from $10cm$ up to $1m$, for an input pump pulse peak power of $1.25kW$. At $10cm$, MI-induced sidebands appear next to the IR pump, and a narrowband SH wave is generated at $532nm$. At $20cm$, the pump spectrum broadens considerably owing to multiple four-wave mixing, and correspondingly the spectrum around $532nm$ also

broadens in a rather symmetric fashion. At $40cm$, the IR spectrum broadening is enhanced by Raman scattering towards the longer wavelengths; this also leads to an asymmetric broadening of the visible spectrum up to about $800nm$. Since the poling and the associated quadratic susceptibility stops at $45cm$, for longer fiber lengths there is no further conversion from the IR to the visible and the main effect is the continuous broadening towards longer wavelength of the IR SC owing to the Raman induced soliton self-frequency shift.

In addition to the output spectra, the numerical simulations also provide the temporal intensity profile of the output fields. For example, Fig. 10 reports a portion of typical temporal profiles of signals generated in the visible range, which exhibit fast sub-picosecond fluctuations. The inset in Fig. 10 shows with a dashed red curve the bandpass filter used to slice the visible spectrum.

5. Conclusions

We have presented a nonlinear single-envelope equation able to model quadratic and cubic ultra-broadband nonlinear dynamics in photonic devices. Owing to a proper formal definition of the complex envelope, it is possible to treat pulses of arbitrary frequency content. A proper definition of the envelope is crucial for second-order nonlinearities, due to the generation of frequency components around zero. Previous works [7, 21], more focused on cubic nonlinearities, did not consider this aspect. We have shown the case of the generation of tunable visible light from large band conversion, in a LBO quadratic crystal, of the infrared continuum from standard photonic crystal fibers. Moreover, we have presented the modeling of a visible supercontinuum

generation, initiated by second-harmonic generation, in a quadratic poled germanium-doped microstructured fiber.

6. Acknowledgments

The present research is supported in Brescia by the Italian Ministry of University and Research (MIUR), grant PRIN 2009P3K72Z and by Fondazione Cariplo, grant n.2010-0595 and grant n.2009-2730.

References

[1] N. Bloembergen, "Nonlinear optics: past, present, and future," IEEE J. Sel. Top. Quantum Electron. **6**, 876-880 (2000).

[2] K. L. Vodopyanov, O. Levi, P. S. Kuo, T. J. Pinguet, J. S. Harris, M. M. Fejer, B. Gerard, L. Becouarn, and E. Lallier,"Optical parametric oscillation in quasi-phase-matched GaAs," Opt. Lett. **29**, 1912-1914 (2004).

[3] C. R. Phillips and M. M. Fejer,"Stability of the singly resonant optical parametric oscillator," J. Opt. Soc. Am. B **27**, 2687-2699 (2010).

[4] O. Levi, T. J. Pinguet, T. Skauli, L. A. Eyres, K. R. Parameswaran, J. S. Harris, Jr., M. M. Fejer, T. J. Kulp, S. E. Bisson, B. Gerard, E. Lallier, and L. Becouarn, "Difference frequency generation of 8-m radiation in orientation-patterned GaAs," Opt. Lett. **27**, 2091-2093 (2002).

[5] P. Maddaloni, P. Malara, G. Gagliardi, and P. De Natale,"Mid-infrared fibre-based optical comb," New J. Phys. **8**, 262-269 (2006).

[6] F. Junginger, A. Sell, O. Schubert, B. Mayer, D. Brida, M. Marangoni, G. Cerullo, A. Leitenstorfer, and R. Huber, "Single cycle multiterahertz transients with peak fields above 10MV/cm," Opt. Lett. **35**, 2645-2647 (2010).

[7] J. M. Dudley, G. Genty, and S. Coen,"Supercontinuum generation in photonic crystal fiber," Rev. Mod. Phys. **78**, 1135-1184 (2006).

[8] J. Price, T. Monro, H. Ebendorff-Heidepriem, F. Poletti, P. Horak, V. Finazzi, J. Leong, P. Petropoulos, J. Flanagan, G. Brambilla, X. Feng,

and D. Richardson, "Mid-IR Supercontinuum Generation From Nonsilica Microstructured Optical Fibers,"IEEE J. Sel. Top. Quantum Electron. **13**, 738-749 (2007).

[9] C. Langrock, M. M. Fejer, I. Hartl, and M. E. Fermann, "Generation of octave-spanning spectra inside reverse-proton-exchanged periodically poled lithium niobate waveguides," Opt. Lett. **32**, 2478-2480 (2007).

[10] T. R. Schibli, I. Hartl, D. C. Yost, M. J. Martin, A. Marcinkevicius, M. E. Fermann, and J. Ye, "Optical frequency comb with sub-mHz linewidth and $>$ 10 W average power," Nat. Photon. **2**, 355-359 (2008).

[11] R. R. Alfano, and S. L. Shapiro, "Observation of selfphase modulation and small-scale filaments in crystals and glasses," Phys. Rev. Lett. **24**, 592-594 (1970).

[12] J. K. Ranka, R. S. Windeler, and A. J. Stenz, "Visible continuum generation in air-silica microstructure optical fibers with anomalous dispersion at 800 nm," Opt. Lett. **25**, 25-27 (2000).

[13] J. C. Knight, "Photonic crystal fibres," Nature **424**, 847-851 (2003).

[14] P. St. J. Russell, "Photonic crystal fibres," Science **299**, 358-362 (2003).

[15] M. Conforti, F. Baronio, and C. De Angelis, "From femtosecond infrared to picosecond visible pulses: temporal shaping with high-efficiency conversion," Opt. Lett. **32**, 1779-1781 (2007).

[16] U. Sapaev and G. Assanto, "Femtosecond pulse synthesis by efficient

second-harmonic generation in engineered quasi phase matching gratings," Opt. Express **15**, 7488-7457 (2007).

[17] M. Conforti, F. Baronio, C. De Angelis, G. Sanna, D. Pierleoni, and P. Bassi, "Spectral shaping of femtoseond pulses in aperiodic quasi-phase-matched gratings," Opt. Comm. **281**, 1693-1698 (2008).

[18] M. Marangoni, D. Brida, M. Conforti, A. D. Capobianco, C. Manzoni, F. Baronio, G. F. Nalesso, C. De Angelis, R. Ramponi, and G. Cerullo, "Synthesis of picosecond pulses by spectral compression and shaping of femtosecond pulses in engineered quadratic nonlinear media," Opt. Lett. **34**, 241-243 (2009).

[19] M. Marangoni, G. Sanna, D. Brida, M. Conforti, G. Cirmi, C. Manzoni, F. Baronio, P. Bassi, C. De Angelis, G. Cerullo, "Observation of spectral drift in engineered quadratic nonlinear media," Appl. Phys. Lett. **93**, 021107(1-3) (2008).

[20] T. Brabec and F. Krausz, "Nonlinear optical pulse propagation in the single-cycle regime," Phys. Rev. Lett. **78**, 3282-3285 (1997).

[21] T. Brabec and F. Krausz, "Intense few-cycle laser fields: Frontiers of nonlinear optics," Rev. Mod. Phys. **72**, 545-591 (2000).

[22] A. V. Housakou and J. Herrmnann, "Supercontinuum generation of higher-order solitons by fission in photonic crystal fibers," Phys. Rev. Lett. **87**, 203901 (2001).

[23] P. Kinsler, "Optical pulse propagation with minimal approximations," Phys. Rev. A **81**, 013819 (2010).

[24] M. Conforti, F. Baronio, and C. De Angelis, "Nonlinear envelope equation for broadband optical pulses in quadratic media," Phys. Rev. A **81**, 053841(1-4) (2010).

[25] M. Conforti, F. Baronio, and C. De Angelis, "Utra-broadband optical phenomena in quadratic nonlinear media," IEEE Photon. J. **2**, 600-610 (2010).

[26] S. Haykin, *Communication System, 4th ed.*, (John Wiley & Sons, 2001).

[27] M. Conforti, F. Baronio, C. De Angelis, M. Marangoni, and G. Cerullo, "Theory and experiments on multistep parametric processes in nonlinear optics," J. Opt. Soc. Am. B **28**, 892-895 (2011).

[28] V.V. Kozlov and S. Wabnitz, "Harmonic and supercontinuum generation in quadratic and cubic nonlinear optical media," J. Opt. Soc. Am. B **27**, 1707-1711 (2010).

[29] C. R. Phillips, C Langrock, J. S. Pelc, M. M. Fejer, I. Hartl, and M. E. Fermann, "Supercontinuum generation in quasi-phasematched waveguides," Opt. Express **19**, 18754-18773 (2011).

[30] M. Conforti, F. Baronio, and C. De Angelis, "Modelling of ultrabroadband and single-cycle phenomena in anisotropic quadratic crystals," J. Opt. Soc. Am. B **28**, 1231-1237 (2011).

[31] M.R.A. Moghaddam, S.W. Harun, R. Akbari, and H. Ahmad, "Flatly broadened supercontinuum generation in nonlinear fibers using a mode locked bismuth oxide based erbium doped fiber laser," Laser Phys. Lett. **8**, 369-375 (2011).

[32] C. Lesvigne,V. Couderc, A. Tonello, P. Leproux, A. Barthelemy, S. Lacroix, F. Druon, P. Blandin, M. Hanna, and P. Georges, "Visible supercontinuum generation controlled by intermodal four-wave mixing in microstructured fiber," Opt. Lett. **32**, 2173-2175 (2007).

[33] R. Buczynski, D. Pysz, R. Stepien, A.J. Waddie, I. Kujawa, R. Kasztelanic, M. Franczyk, and M.R. Taghizadeh, "Supercontinuum generation in photonic crystal fibers with nanoporous core made of soft glass," Laser Phys. Lett. **8**, 443-448 (2011).

[34] J.C. Travers, A.B. Rulkov, B.A. Cumberland, S.V. Popov and J.R. Taylor, "SNon-linear applications of microstructured optical fibres," Opt. Quant. Electron. **39**, 963-974 (2007).

[35] Y. Fujii, B.S. Kawasaki, K.O. Hill, and D.C. Johonson, "Sum-frequency light generation in optical fibers," Opt. Lett. **5**, 48-50 (1980).

[36] U. Osterberg and W. Margulis "Experimental studies on efficient frequency doubling in glass optical fibers," Opt. Lett. **12**, 57-59 (1987).

[37] P.A. Champert, V. Couderc, P. Leproux, S. Fevrier, V. Tombelaine, L. Labonte, P. Roy, and C. Froehly, "White-light supercontinuum generation in normally dispersive optical fiber using original multi-wavelength pumping system," Opt. Express **12**, 4366-4371 (2004).

[38] V. Tombelaine, C. Buy-Lesvigne, P. Leproux, V. Couderc, and G. Melin, "Optical poling in germanium-doped microstructured optical fiber for visible supercontinuum generation," Opt. Lett. **33**, 2011-2013 (2008).

[39] V. Couderc, A. Tonello, C. Buy-Lesvigne, P. Leproux, and L. Grossard, "Unprecedented Raman cascading and four-wave mixing from second-harmonic generation in optical fiber," Opt. Lett. **35**, 145-147 (2010).

Fig. 1. Experimental setup. Nd:YAG laser pump delivering $800ps$ pulses, at $1064nm$, $8kHz$ repetition rate; L1, L2, L3 lenses; $\lambda/2$ half wave plate; P polarizer; F, filter; photonic crystal fiber (PCF); quadratic biaxial LBO crystal; optical spectrum analyzer (OSA).

Fig. 2. Cross-sectional scanning electron microscope image of PCF and calculated group velocity dispersion parameter D.

Fig. 3. Typical SC spectrum at the output of the PCF. Top, OSA meausurement, bottom, numerical trace. Here, input peak power of $7.8kW$.

Fig. 4. Spectrum at the output of the LBO crystal. Top, OSA meausurement, bottom, numerical result. The azimuthal angle $\phi = 0^o$.

Fig. 5. Typical numerical temporal profiles filtered at $700nm$ at the output of the LBO crystal.

Fig. 6. Top, OSA meausurement of visible spectra at the output of the LBO crystal at different crystal azimuthal angles ($\phi = 0^o$, blue line; $\phi = 3^o$, red line; $\phi = 4.5^o$, light blue line). Bottom, parametric gain for second harmonic generation in LBO as a function of generated wavelength and crystal azimuthal angle.

Fig. 7. Cross-sectional scanning electron microscope image of the germanium-doped PCF and calculated group velocity dispersion parameter D.

Fig. 8. OSA measurement of typical spectrum at the output of the germanium-doped PCF. Here, input peak power of $2.5kW$.

Fig. 9. Numerical trace of typical spectrum at different lenghts of the germanium-doped PCF. Here, input peak power of $1.25kW$.

Fig. 10. Portion of numerical temporal profiles filtered around $532nm$ at the output of germanium-doped PCF. Dashed red curve, bandpass filter used to slice the visible spectrum. Here, input peak power of $1.25kW$.

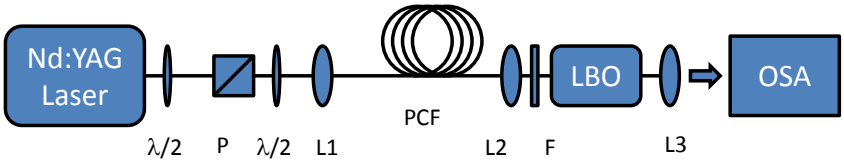

Figure 1: Experimental setup. Nd:YAG laser pump delivering 800ps pulses, at 1064nm, 8kHz repetition rate; L1, L2, L3 lenses; $\lambda/2$ half wave plate; P polarizer; F, filter; photonic crystal fiber (PCF); quadratic biaxial LBO crystal; optical spectrum analyzer (OSA).

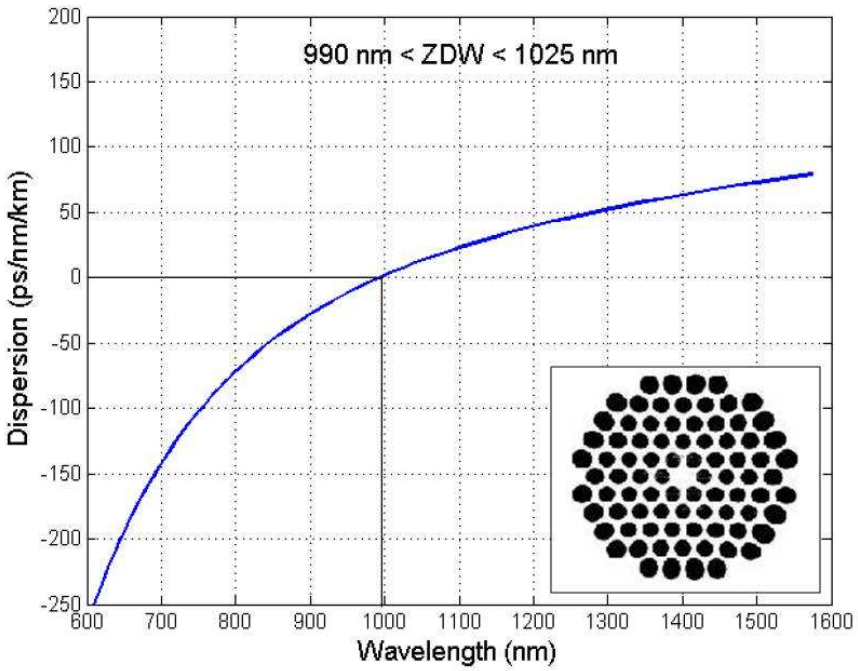

Figure 2: Cross-sectional scanning electron microscope image of PCF and calculated group velocity dispersion parameter D.

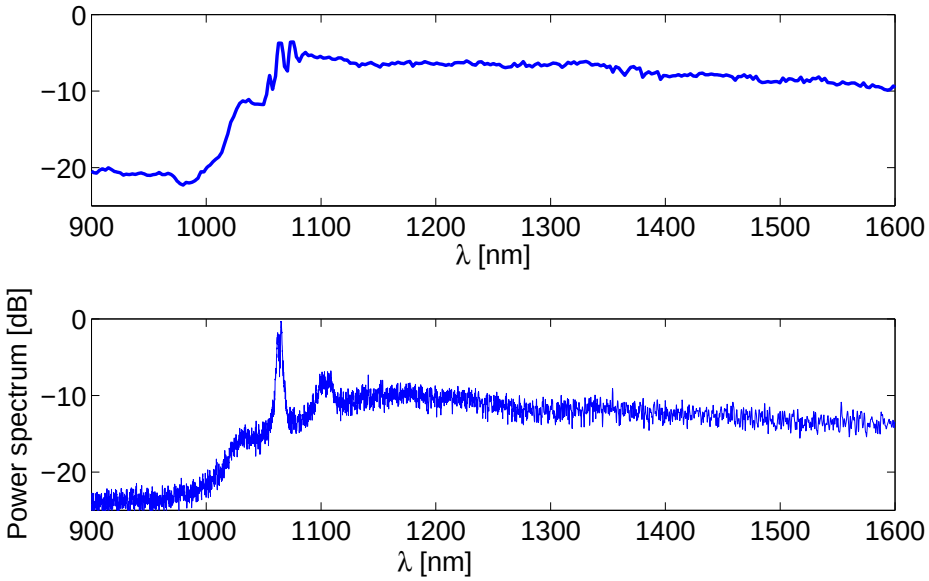

Figure 3: Typical SC spectrum at the output of the PCF. Top, OSA meausurement, bottom, numerical trace. Here, input peak power of $7.8kW$.

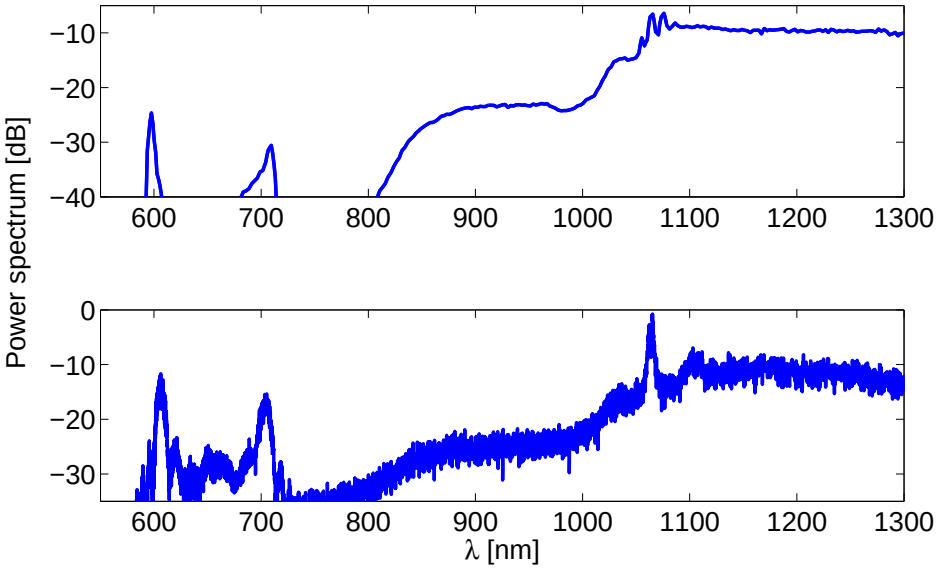

Figure 4: Spectrum at the output of the LBO crystal. Top, OSA meausurement, bottom, numerical result. The azimuthal angle $\phi = 0^o$.

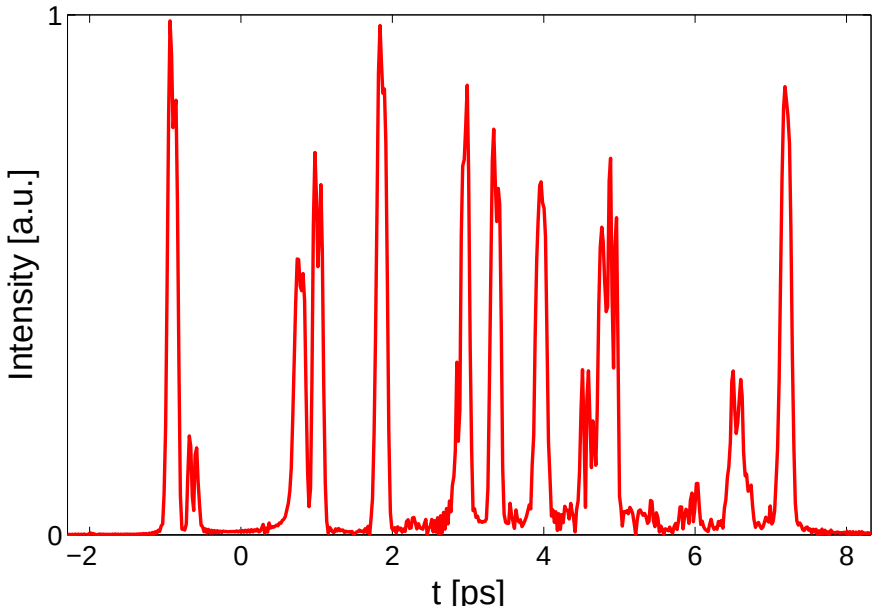

Figure 5: Typical numerical temporal profiles filtered at $700nm$ at the output of the LBO crystal.

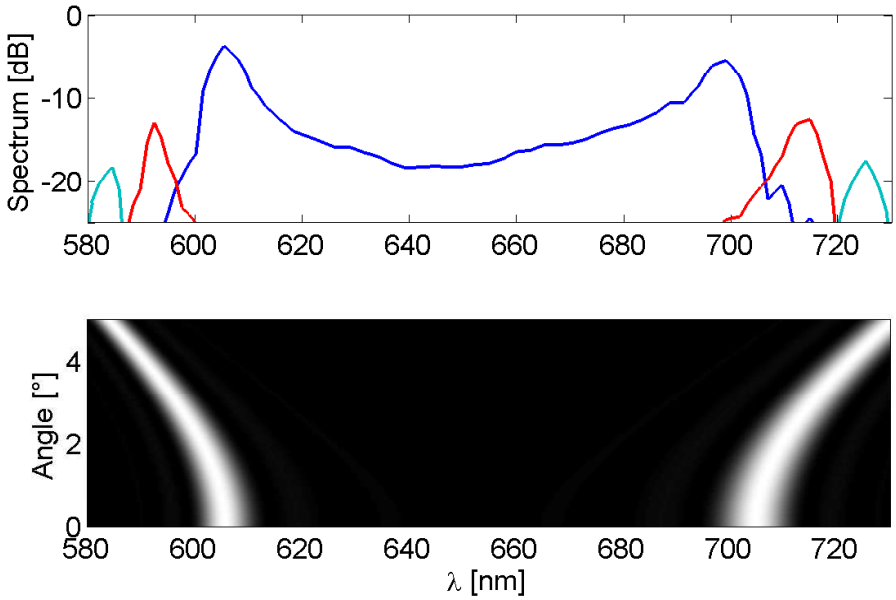

Figure 6: Top, OSA meausurement of visible spectra at the output of the LBO crystal at different crystal azimuthal angles ($\phi = 0^o$, blue line; $\phi = 3^o$, red line; $\phi = 4.5^o$, light blue line). Bottom, parametric gain for second harmonic generation in LBO as a function of generated wavelength and crystal azimuthal angle.

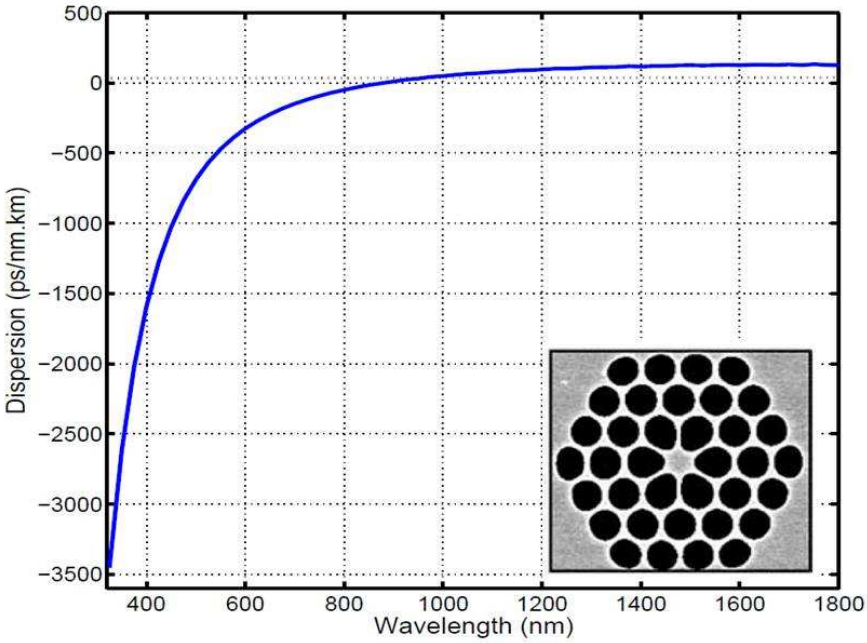

Figure 7: Cross-sectional scanning electron microscope image of the germanium-doped PCF and calculated group velocity dispersion parameter D

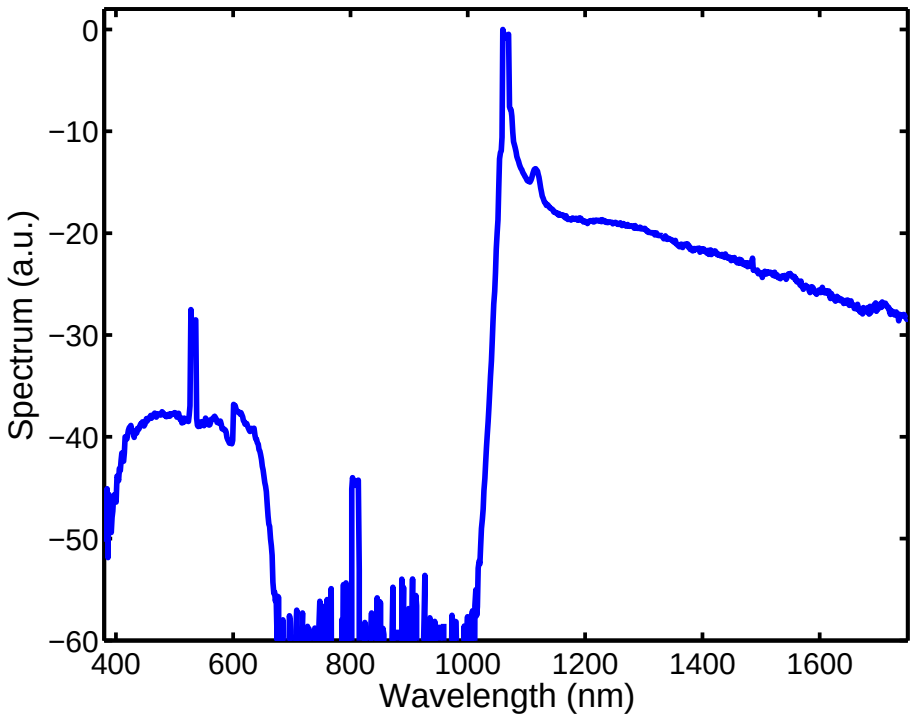

Figure 8: OSA measurement of typical spectrum at the output of the germanium-doped PCF. Here, the input peak power is $2.5kW$.

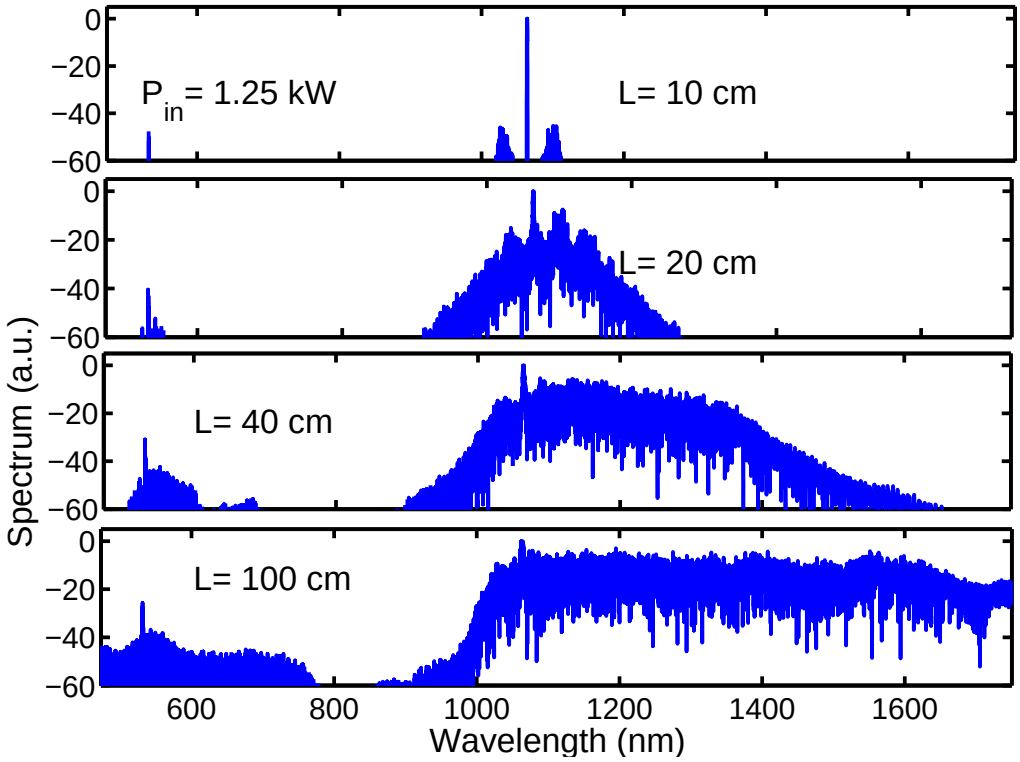

Figure 9: Numerical trace of typical spectrum at different lenghts of the germanium-doped PCF. Here, the input peak power is $1.25kW$.

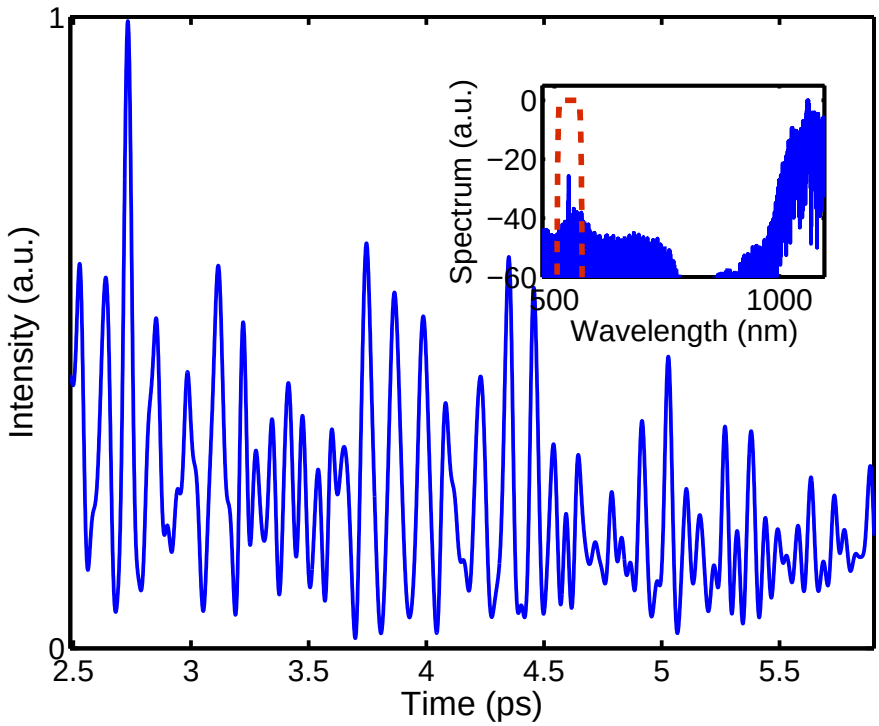

Figure 10: Portion of numerical temporal profiles filtered around $532nm$ at the output of germanium-doped PCF. Dashed red curve, bandpass filter used to slice the visible spectrum. Here, input peak power of $1.25kW$.